INTERNATIONAL JOURNAL OF CLIMATOLOGY
Int. J. Climatol. **30**: 643–657 (2010)
Published online 17 April 2009 in Wiley InterScience
(www.interscience.wiley.com) DOI: 10.1002/joc.1910

RMetS
Royal Meteorological Society

On the interannual wintertime rainfall variability in the Southern Andes

M. H. González* and C. S. Vera

Centro de Investigaciones del Mar y la Atmósfera (CONICET-UBA), Departamento de Ciencias de la Atmósfera y los Océanos, FCEyN, Universidad de Buenos Aires, Buenos Aires, Argentina

ABSTRACT: The paper concentrates on the analysis of the interannual variability of wintertime rainfall in the Southern Andes. Besides the socio-economic relevance of the region, mainly associated with hydroelectric energy production, the study of the climate variability in that area has not received as much attention as others along the Andes. The results show that winter rainfall explains the largest percentage of regional total annuals. A principal component analysis (PCA) of the winter rainfall anomalies showed that the regional year-to-year variability is mostly explained by three leading patterns. While one of them is significantly associated with both the El Niño Southern Oscillation (ENSO), and the Southern Annular Mode (SAM), the other two patterns are significantly related to interannual changes of the sea surface temperature (SST) anomalies in the tropical Indian Ocean. Specifically, changes in the ocean surface conditions at both tropical basins induce in the atmospheric circulation the generation of Rossby wave trains that extend along the South Pacific towards South America, and alter the circulation at the region under study. The relationship between variability in the Indian Ocean and the Andes climate variability has not been previously addressed. Therefore, this result makes a significant contribution to the identification of the sources of predictability in South America with relevant consequences for future applications in seasonal predictions. Copyright © 2009 Royal Meteorological Society

KEY WORDS interannual variability; El Niño Southern oscillation; Southern annular mode; Indian Ocean; Southern Andes

Received 29 January 2008; Revised 12 December 2008; Accepted 3 March 2009

1. Introduction

The Andes Mountains extend all along the west coast of South America, which encompasses several important socio-economic activities for the countries involved. South of 35 °S, the orographic region is of particular relevance for the economies of Argentina and Chile because most of the energy resources of both countries come from the hydroelectric generating centres operating in the region. It is therefore evident that such energy production, as well as the regional water availability, is highly sensitive to the regional climate variability.

In the border between Argentina and Chile two different regimes can be identified. Approximately north of 38 °S, the mountains are above 3000 m and prevent the access of humidity from the Pacific Ocean eastwards. South of 38 °S, the mountain height decreases to 1500 m, which allows the incursion of the moist air from the Pacific Ocean to the east of the Andes. At these latitudes, westerly mean flow prevails all year around, being more intense during winter. Owing to the interaction of the mean flow with the orography, maximum precipitation takes place in the vicinity of the mountains, while it decreases eastwards over the Patagonian region. In this dry region, the availability of drinking water is scarce, and generally the rivers starting in the Andes that flow towards the Atlantic Ocean are the most important fresh water sources. In that sense, river runoff in the region is highly dependent on the actual rainfall and snow accumulated in the Andes Mountains.

This region of the Andes exhibits an important interannual rainfall variability that has been partially associated with the El Niño-Southern Oscillation (ENSO) by many authors. During negative phases of the Southern Oscillation Index (SOI), winter precipitation is greater than normal in central Chile (Aceituno, 1988), which also has an impact on the rivers flowing towards the Pacific Ocean (Aceituno and Garreaud, 1995). In addition, a greater number of blocking events have been observed over the South Pacific during warm ENSO events which enhances winter precipitation over the central Andes (Rutllant and Fuenzalida, 1991; Montecinos and Aceituno, 2003). Compagnucci and Vargas (1998) show that winters that precede a mature phase of El Niño (La Niña) are characterized by larger (smaller) amounts of snow over the Andes, north of 36 °S, which contribute to increase (decrease) the water volume of the rivers. On the other hand, positive correlations between the SOI and precipitation rate anomalies between 45 °S and 55 °S have been found by Schneider and Gies (2004). Precipitation decreases there by about 15% during strong El Niños. Compagnucci and Araneo (2005) detected that the

* Correspondence to: M. H. González, CIMA 2° piso-Pabellon II Ciudad Universitaria – 1428-Cdad. Autónoma de Buenos Aires (CABA), Buenos Aires, Argentina. E-mail: gonzalez@cima.fcen.uba.ar

interannual variability of river discharges along the Andes is also influenced by variations in the Pacific Ocean surface conditions not necessarily associated with ENSO.

The motivation of this paper is to better understand the interannual variability of wintertime seasonal rainfall between 37 °S and 43 °S along the Andes. A specific objective of this study is to diagnose how the rainfall anomaly interannual variability in that area is related to interannual changes of both atmospheric circulation anomalies in the Southern Hemisphere (SH) and sea surface temperature (SST) anomalies at the tropical regions, besides those associated with ENSO. The paper is organized as follows: Section 2 describes the dataset and the area of interest. Section 3 presents the rainfall climatological features in the region, while Section 4 discusses the leading patterns of rainfall interannual variability and their associated regional and hemispheric circulation as well as SST anomaly patterns. Section 5 discusses the relevance of the large-scale influence onto the rainfall variability and Section 6 presents the main conclusions.

2. Data and methodology

Monthly rainfall data derived from a selected group of stations from the National Meteorological Service and the Secretary of Hydrology of Argentina have been used in this study. The stations are located in the Southern Andes region between 37 °S and 43 °S, encompassing the Argentinean provinces of Neuquen and Rio Negro (Figure 1). The period of study goes from 1975 to 1997. The analysis concentrates on the seasonal rainfall, the seasons being those determined for the SH.

Monthly SST, 500-hPa geopotential heights (GH), zonal (u) and meridional (v) winds at 700 hPa from National Center of Environmental Prediction (NCEP) reanalysis were also used (Kalnay *et al*. 1996). Monthly anomalies were determined by removing the climatological monthly means. The linear long-term trend was also removed.

The leading patterns of rainfall variability on seasonal time scales were obtained through a principal component analysis (PCA) in the T-mode (Green, 1978). Therefore, the principal scores (PC) describe the spatial patterns, while the loadings provide the temporal evolution of the patterns. The dominant frequencies related with the variability of the leading patterns were identified through spectral analyses. Lagged correlation maps between the loading of the leading patterns and some meteorological variables were computed in order to improve the physical interpretation of the leading patterns.

3. Climatology

The main features of the mean annual rainfall cycle are discussed in this section. Figure 2 shows that the climatological mean rainfall peaks in late autumn and early winter along the whole region. Although the selected area

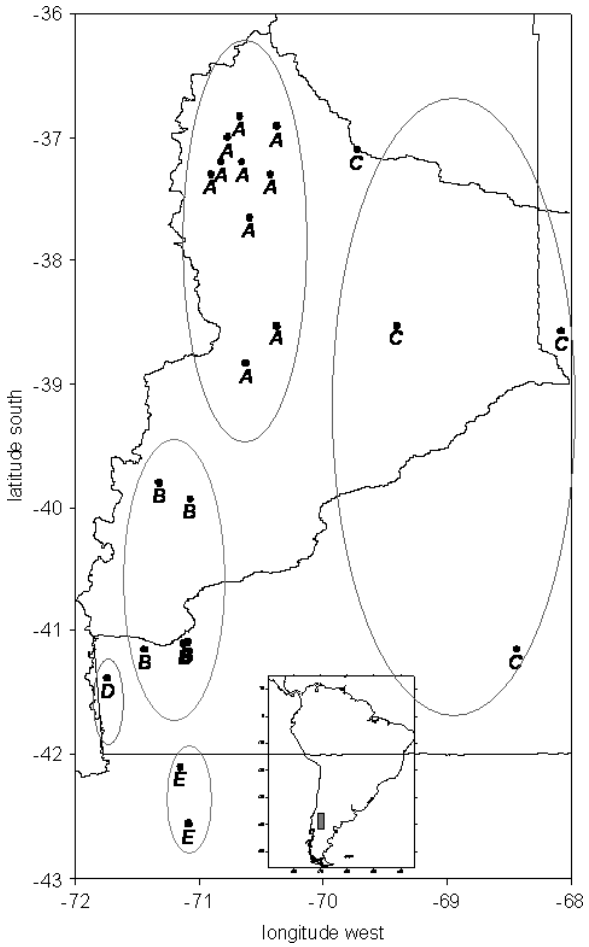

Figure 1. Location of rainfall gauge stations in the study region, categorized into five sub-regions.

is very small (less than 120 000 km^2), the presence of the complex orographic barrier results in large regional inhomogeneities in the mean annual cycle. Figure 2 shows over and near the Andes (A and B) a marked annual cycle, with a wet season in winter being evident with larger amounts in the south (B) than in the north (A). Eastward, much less rainfall characterizes the mean seasonal cycle (C). On the other hand, a super-humid region is observed within the Andes Mountains (D), due to local orographic effects, with a maximum in winter that almost duplicates that observed eastward (Region B). Such a maximum was previously registered by Hoffman (1975) who used more than 1700 stations to compile a detailed climatology of precipitation in South America. Unfortunately, there are no other stations currently operating in that particular area. Rainfall is scarce to the southwest (E), and it shows almost no distinctive annual cycle.

4. Rainfall interannual variability

4.1. Leading patterns

The interannual variability of rainfall anomalies for May, June and July (MJJ, etc. hereafter) is analysed in this section, as it corresponds in general to the rainiest season of

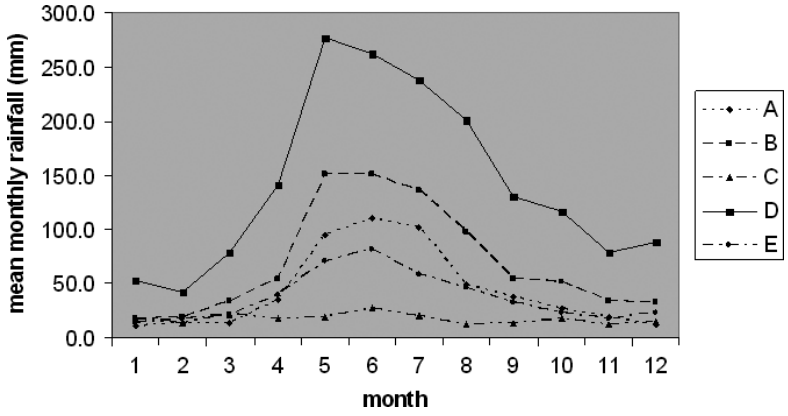

Figure 2. Mean rainfall annual cycle in each of the five regions described in Figure 1.

the region. A PCA was applied to MJJ rainfall anomalies for the period 1975–1997. Four leading patterns were retained following the Kaiser's criterion (Kaiser, 1958), where eigenvalues greater than 1 are considered, and also the scree test (Cattel, 1966), where a break in the slope of plotted eigenvalues is used to determine the quantity of PCs to be analysed. As was discussed in the previous section, the presence of such a complex orographic system promotes the determination of relatively small regions with significantly different climate variability features. In agreement, Zheng and Renwick (2003, and references therein) determine for seasonal prediction purposes six regions in New Zealand, which has a mountain systems as complex as is analysed in the present work, but over a smaller area.

The first two leading patterns (PC1, PC2) explain 26 and 22%, respectively, of the variance, both being statistically significant. Figure 3 shows that PC1 has the strongest influence in the southwest, while PC2 mostly describes the variability of anomalies of opposite sign in the central region along the east–west direction. PC3 exhibits the largest amplitudes over a void data region and therefore is not considered in the study. On the other hand, the fourth pattern (PC4), although it explains only 8% of the variance, is analysed here, as it depicts the variability in the northern region.

A spectrum analysis for the loadings of PC1, PC2 and PC4 is presented in Figure 4 in order to identify the dominant periods of variability. The labelled peaks correspond to those significant at 95% confidence level of a white noise test (Conrad and Pollack, 1950). A peak at around 2 years is detected for PC1 and PC2, while a 4.4-year periodicity is also found in the PC1 spectrum (Figure 4(a) and (b)). It is speculated that both peaks of variability might be related to those observed by other authors (e.g. Mo, 2000) in the interannual variability of the SST anomalies over the tropical Indian and Pacific Oceans as is further discussed in the following sections. PC2 also exhibits maximum variability at around 20 years. Nevertheless, considering that such a period is similar to that of the database record, this peak might be associated with trends or variability on lower frequencies not fully removed by the filtering technique applied. On the other hand, PC4 exhibits peaks of variability at around 3 and 5.5 years (Figure 4(c)). As described in the next sections, those peaks might be explained by the fact that PC4 variability is related to ENSO and the Southern Annular Mode (SAM), which exhibit peaks of variability at around those two periods (e.g. Mo, 2000).

4.2. Regional analysis

The circulation anomalies associated with the leading patterns of rainfall anomaly variability are explored in order to identify the key elements of the regional circulation that promote or inhibit rainfall anomalies in the region. Correlation maps were made between the PC time series and the MJJ seasonal anomalies of 500-hPa geopotential heights, which describe the regional patterns of circulation. Similar maps were also made for zonal and meridional wind anomalies at 700 hPa, indicative of the low-level flow across the Andes, transporting moisture in the region.

It is well known that mean moisture transport along the Southern Andes is related to low-level westerly winds (e.g. Schwerdtfeger, 1975). Nevertheless, the analysis for each of the PCs shows that zonal wind anomalies are embedded in different regional circulation anomaly patterns. Positive winter rainfall anomalies in southwestern region (PC1) are associated with westerly and southerly wind anomalies (Figures 5(b) and (c)), which in turn are promoted by an anticyclonic anomaly centred off the western coast of South America and a cyclonic anomaly centre over southern Brazil (Figure 5(a)). On the other hand, westerly zonal wind anomalies and northerly meridional wind anomalies at lower levels (Figure 6(b) and (c)), related to positive phases of PC2, are associated with a cyclonic anomaly centred in southeastern Pacific, at around 85 °W, 45 °S (Figure 6(a)). Compagnucci and Araneo (2005) showed that positive discharge anomalies in the rivers of the region are associated with a high frequency of cyclonic systems from the Pacific eastward. As further discussed in Section 4.3, the regional circulation anomalies seem to be part of a Rossby wave-train pattern extended between the western South Pacific and South America, which in turn is forced by changes in the SST anomalies at the Indian Ocean.

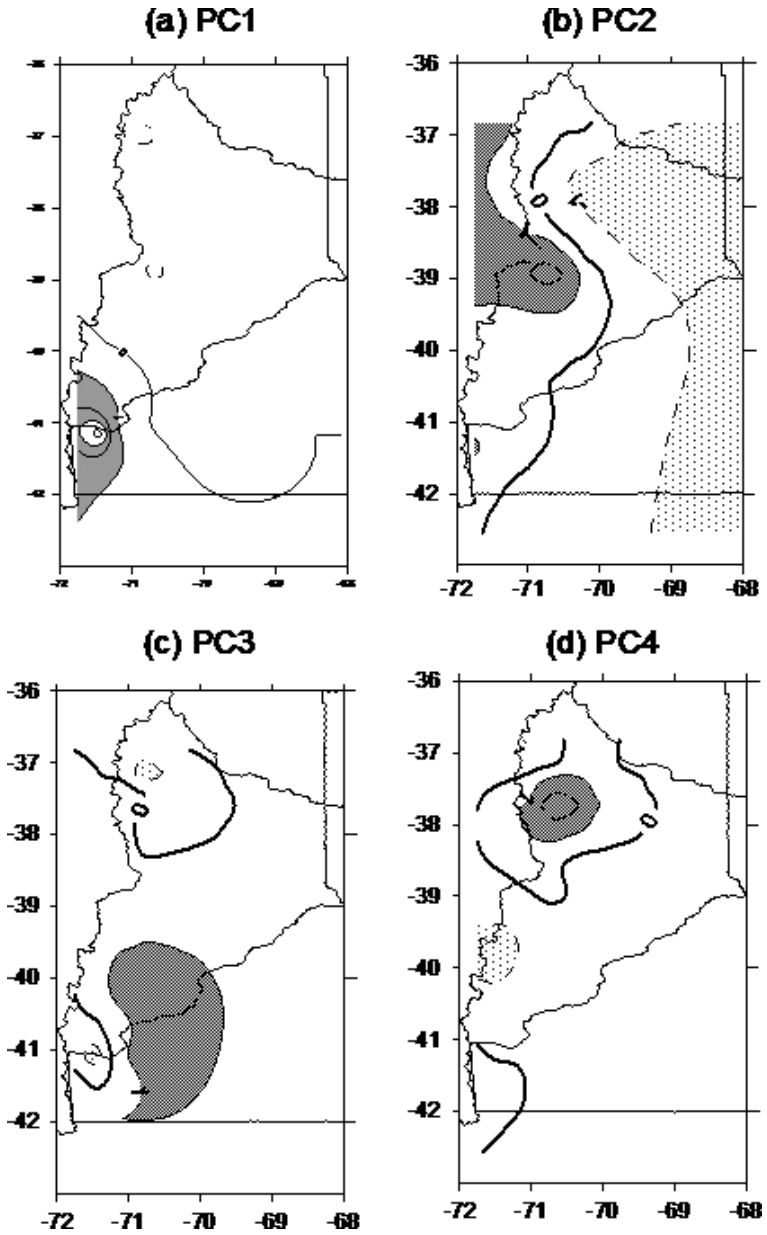

Figure 3. Leading patterns of MJJ accumulated rainfall anomalies for the period 1975–1997. Negative (positive) contours are dashed (full). Values larger than 1 mm day^{-1} are shaded in dark grey, and less than -1 mm are shaded in light grey.

Positive rainfall anomalies in the northern portion of the region (PC4) are related with an anticyclonic anomaly located right over the orography (Figure 7(a)). It is noticeable that negligible correlation values between PC4 time series and low-level zonal wind anomalies are observed (Figure 7(b)), while moderate relationships are depicted with negative meridional wind anomalies (Figure 7(c)). This result might suggest that moist air is transported along the eastern slope of the Andes from the tropical areas into the region of interest.

4.3. Hemispherical analysis

The section explores the relationship between the large-scale anomaly patterns in both the atmosphere and oceans and the rainfall anomaly variability in the region. The existence of such relationships might provide useful hints to improve the seasonal predictions.

Lagged correlation maps between PC1 time series and both SST and 500-hPa geopotential height anomalies were performed, which are displayed in Figures 8 and 9. Negative correlation values along the tropical band with extreme values in the Indian Ocean (5 °S–20 °S; 60 °E–90 °E) are detected between FMA SST anomalies and MJJ PC1 (Figure 8(a)). This pattern persists for MAM SST anomalies (Figure 8(b)), whereas it weakens for the corresponding anomalies of AMJ (Figure 8(c)) and MJJ (Figure 8(d)). Evidences of the influence of Indian Ocean conditions on the climate variability have been previously documented for other regions in the SH. Zheng and Frederiksen (2006) demonstrated that SST conditions in central Indian Ocean in MAM are a good

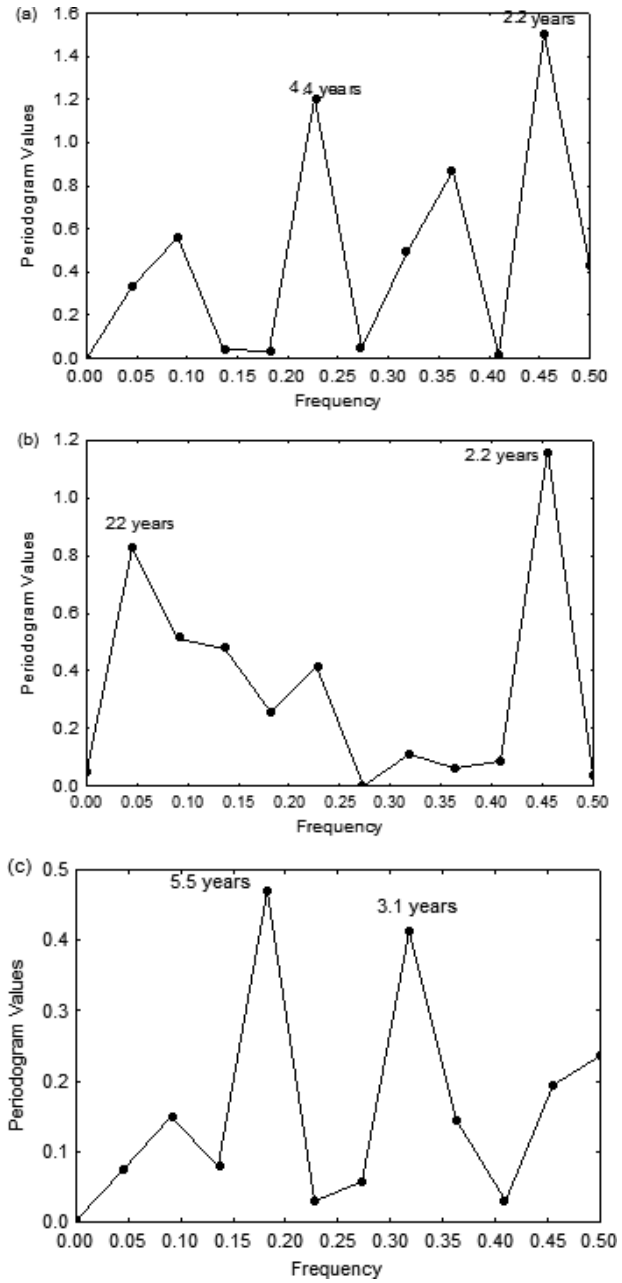

Figure 4. A spectrum analysis of the loadings of PC1, PC2 and PC4; the labelled peaks correspond to those significant at 95% confidence level of a white noise test.

predictor of winter rainfall variability in New Zealand. Reason (2001) described links between Indian Ocean SST variability and rainfall in Southern Africa. However, there are no previous studies showing the links between the variability of the SST anomalies in tropical Indian Ocean and that of the climate in extra-tropical South America.

The correlation map between the 500-hPa geopotential height anomalies for FMA and the MJJ PC1 (Figure 9(a)) shows a wave train extending from Australia towards South America. The wave-like pattern is also evident for the other three analysed lags, MAM (Figure 9(b)), AMJ (Figure 9(c)) and MJJ (Figure 9(d)). The wave-like pattern resembles that associated with the third leading pattern of circulation interannual variability in the SH, known as Pacific South American Pattern 2 (PSA2). Mo (2000) shows that PSA2 is characterized by a wave train emanating from the tropical western Pacific polewards, and it is associated with the tropical Indian Ocean SST anomalies on quasi-biennial time scales (Mo, 2000). Figure 9 also shows that the anticyclonic anomaly centred on the western coast of South America (Figure 5(a)), described in Section 4.2, is part of the large-scale wave-train pattern, and during AMJ it exhibits the largest correlation magnitude with MJJ PC1.

MJJ PC2 variability tends to be related to cold SST anomalies in the Indian Ocean since FMA (Figure 10(a)). That relationship attains its largest magnitude on MAM (Figure 10(b)) and weakens in the subsequent seasons (Figure 10(c) and (d)). Large lagged correlation magnitudes are also observed between MJJ PC2 and SST anomalies at the extra-tropical South Pacific Ocean. The analysis of the large-scale circulation variability associated with PC2 shows for all lags considered a band of negative correlation values extending along the subtropical South Pacific (Figure 11). Zonally oriented wave-like patterns are also discernible at high latitudes. Furthermore, the cyclonic anomaly located off the South American coast in MJJ (Figures 6(a) and 11(d)) seems to get its largest relationship with MJJ rainfall anomalies associated with PC2 during AMJ (Figure 11(c)). Such an anomaly centre is also present in the lagged correlation maps for the previous seasons but located westwards.

The correlation maps between PC4 and lagged SST anomalies display an ENSO-like pattern (Figure 12). Negative SST anomalies in the central equatorial Pacific are related to positive rainfall anomalies in the region of action for PC4 from FMA to MJJ with largest correlation magnitudes by MAM and AMJ.

The correlation maps between 500-hPa geopotential height anomalies and PC4 show an annular-like pattern at high latitudes similar to that associated with the SAM (Mo 2000) combined with wave-like patterns at middle latitudes (Figure 13). Previous work has shown that both ENSO and SAM might have a combined influence on the rainfall variability in some regions of the SH. While Silvestri and Vera (2003) show such influence on precipitation interannual variability in southeastern South America, particularly during spring, Zheng and Frederiksen (2006) show that both signals affect summer rainfall variability in the New Zealand sector. Moreover, Reason and Rouault (2005) have shown that wetter (drier) winters in western South Africa occur during negative (positive) SAM phase. The results presented here confirm that such combined influence of ENSO and SAM can affect also the climate variability in the Southern Andes.

5. Discussion

The previous analysis shows that the rainfall interannual variability across the Southern Andes is strongly related

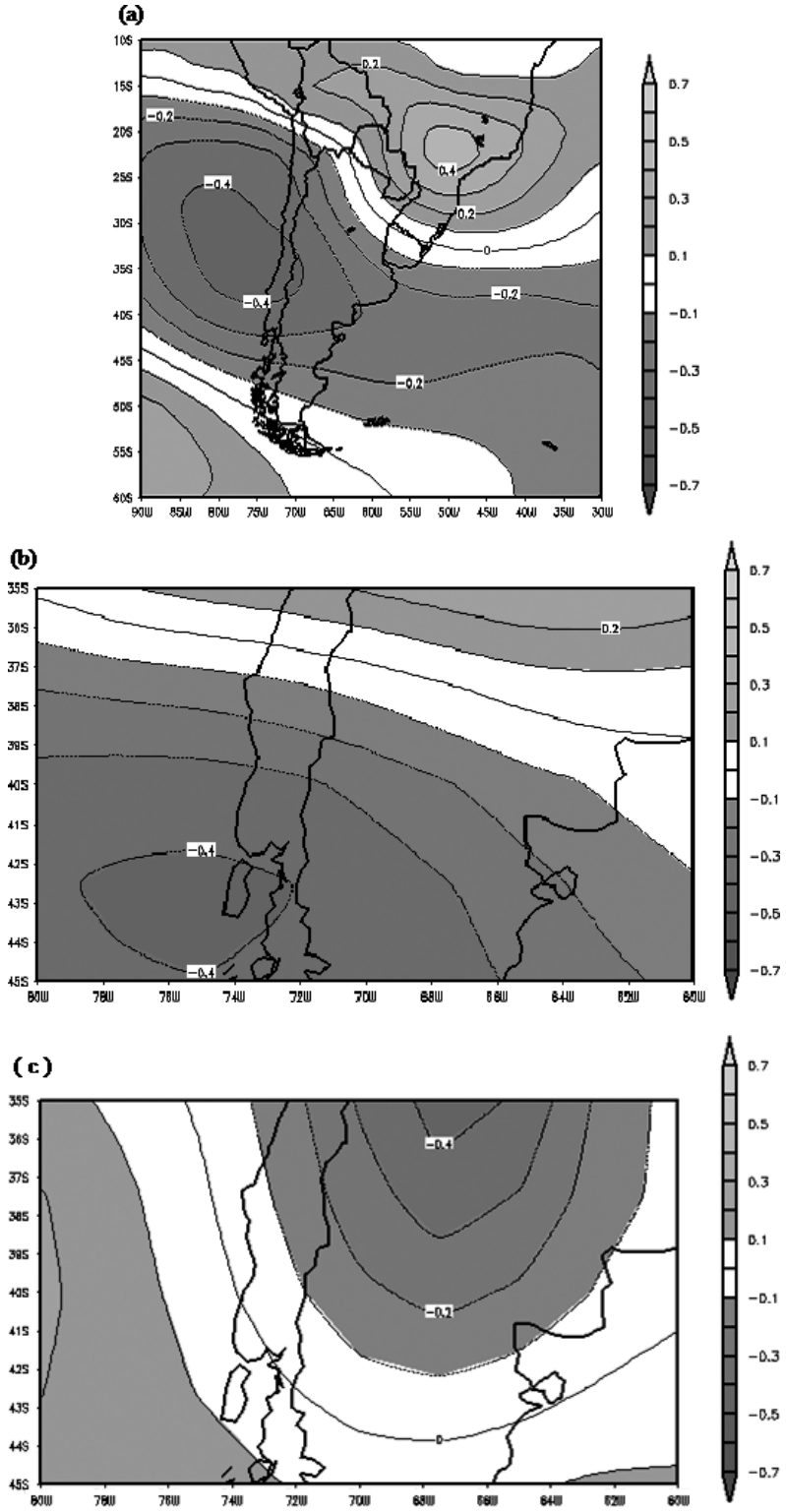

Figure 5. Simultaneous seasonal correlation between MJJ rainfall anomalies PC1 and (a) 500-hPa geopotential height, (b) 700 hPa zonal wind and (c) 700 hPa meridional wind. Values larger than 0.4 correspond to those significant at 95% confidence level.

to the interannual variability of the SST anomalies at tropical Indian and Pacific Oceans. Specifically, changes in the ocean surface conditions at both tropical basins induce in the atmospheric circulation the generation of Rossby wave trains that extend along the South Pacific towards South America and alter the circulation at the region under study.

In addition, the leading pattern of circulation variability in the SH, i.e. the SAM, also seems to have a significant correlation with the year-to-year rainfall variability at the Southern Andes. SAM is associated with intensification and weakening of the westerlies mainly forced by the atmospheric internal variability (e.g. Thompson and Wallace 2000). Therefore, the relationship between the

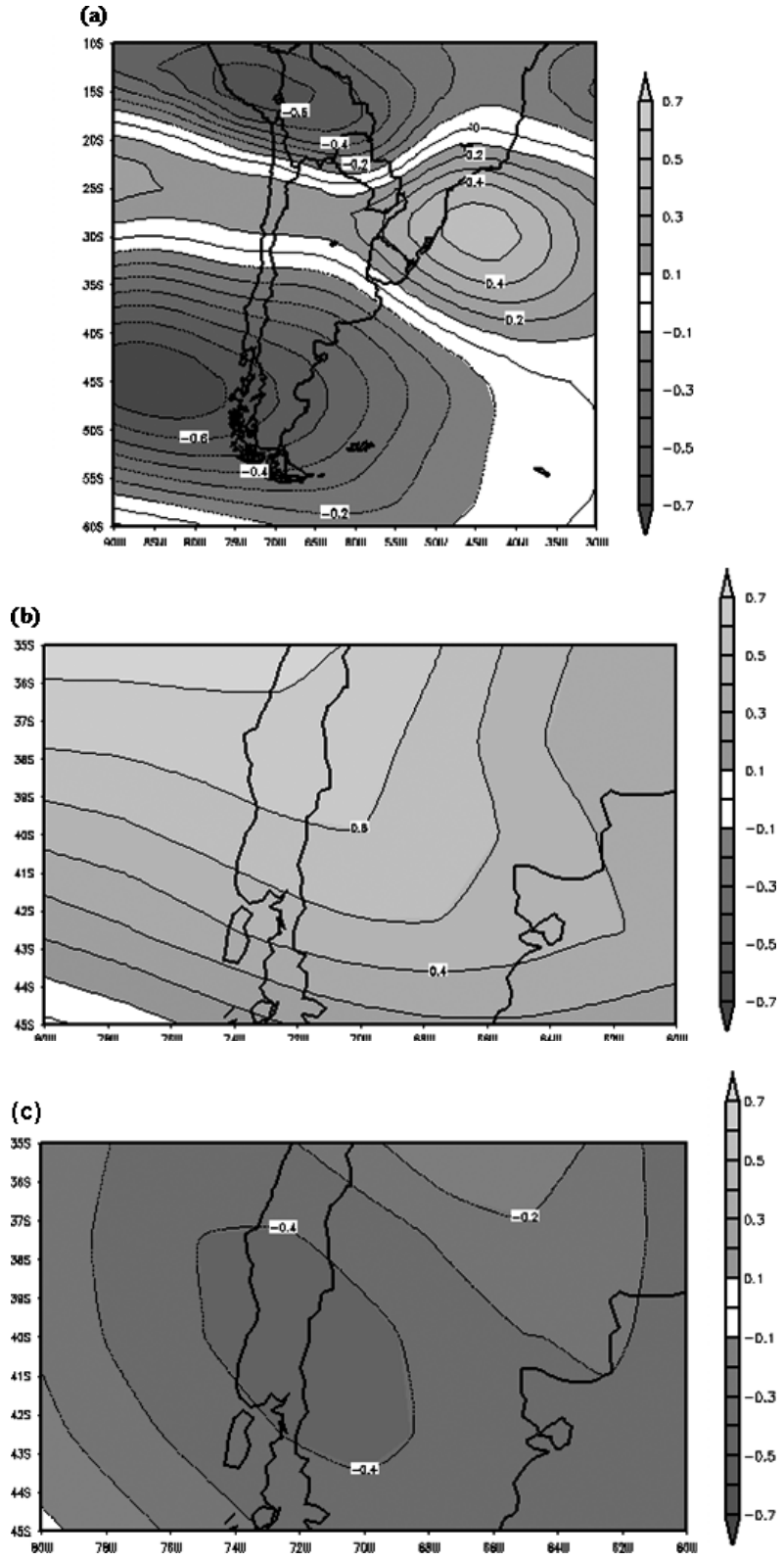

Figure 6. Same as in Figure 5 for MJJ rainfall anomalies PC2.

rainfall variability in Southern Andes and that associated with ENSO, SAM and the SST anomalies at the Indian Ocean is further explored here.

The time series of the SST anomalies in the El Niño-3.4 region (EN3.4) was considered as the ENSO index. The SAM index is determined by the time series of the leading pattern from an empirical orthogonal function (EOF) analysis of monthly mean 700-hPa height anomalies (Mo, 2000). An index representative of the SST variability in the tropical Indian Ocean was quantified by the SST anomalies averaged over the region (5 °S–20 °S, 60 °E–90 °E) (SST-IO).

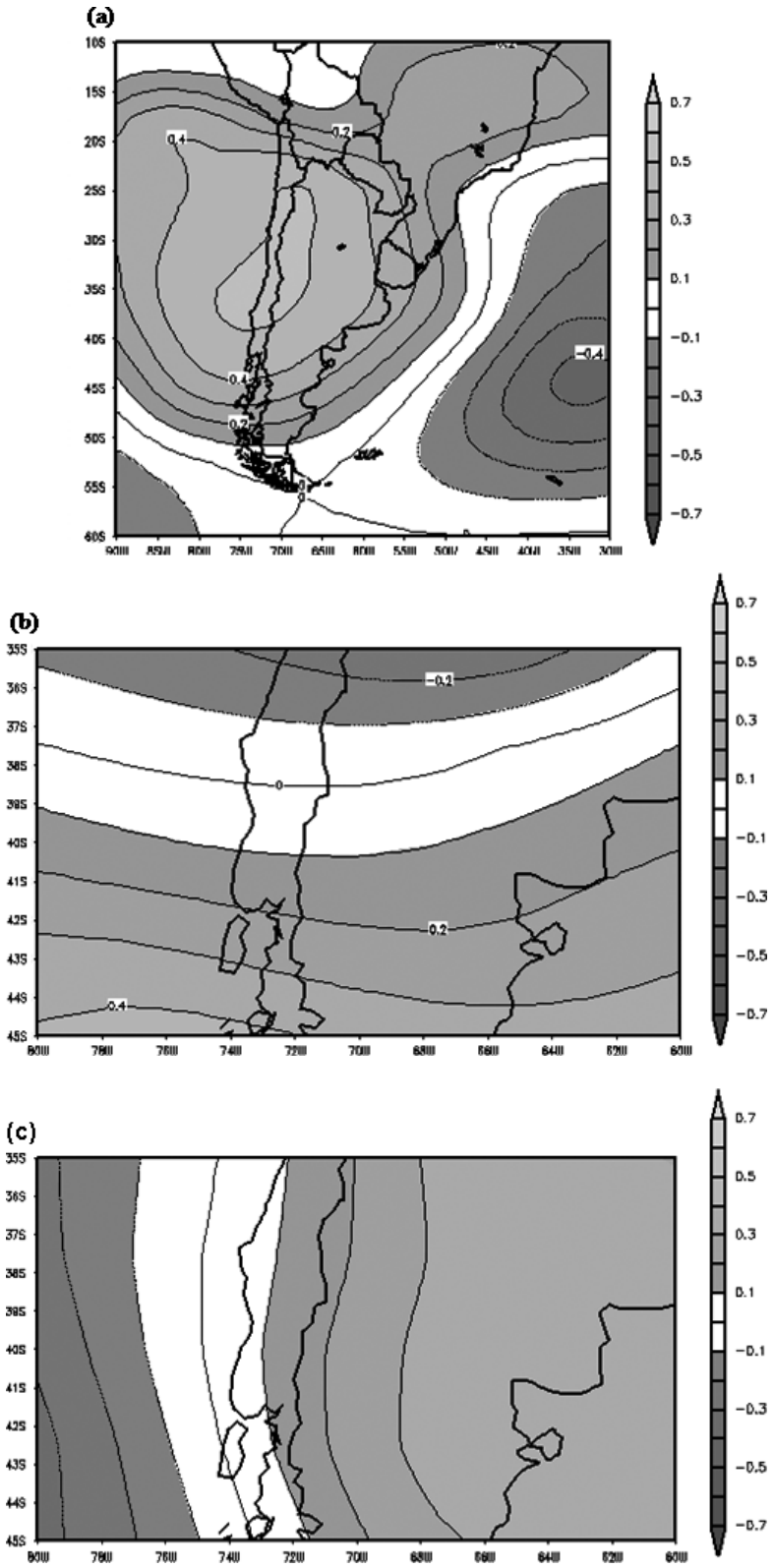

Figure 7. Same as in Figure 5 for MJJ rainfall anomalies PC4.

Table I shows the lagged correlations between the time series of PC1, PC2 and PC4 and the SST-IO, EN3.4 and SAM. A *t*-test was used to evaluate the significance of the correlation values displayed in Table I (Brooks and Carruthers, 1953). Previously, it was checked for each of the time series as to whether there were autocorrelations or not, and it was confirmed that neither of them is significantly auto-correlated.

It is evident that neither of the correlations between the rainfall variability associated with PC1 and the three indices are statistically significant. Nevertheless, both the tropical portions of the Indian and Pacific oceans exhibit

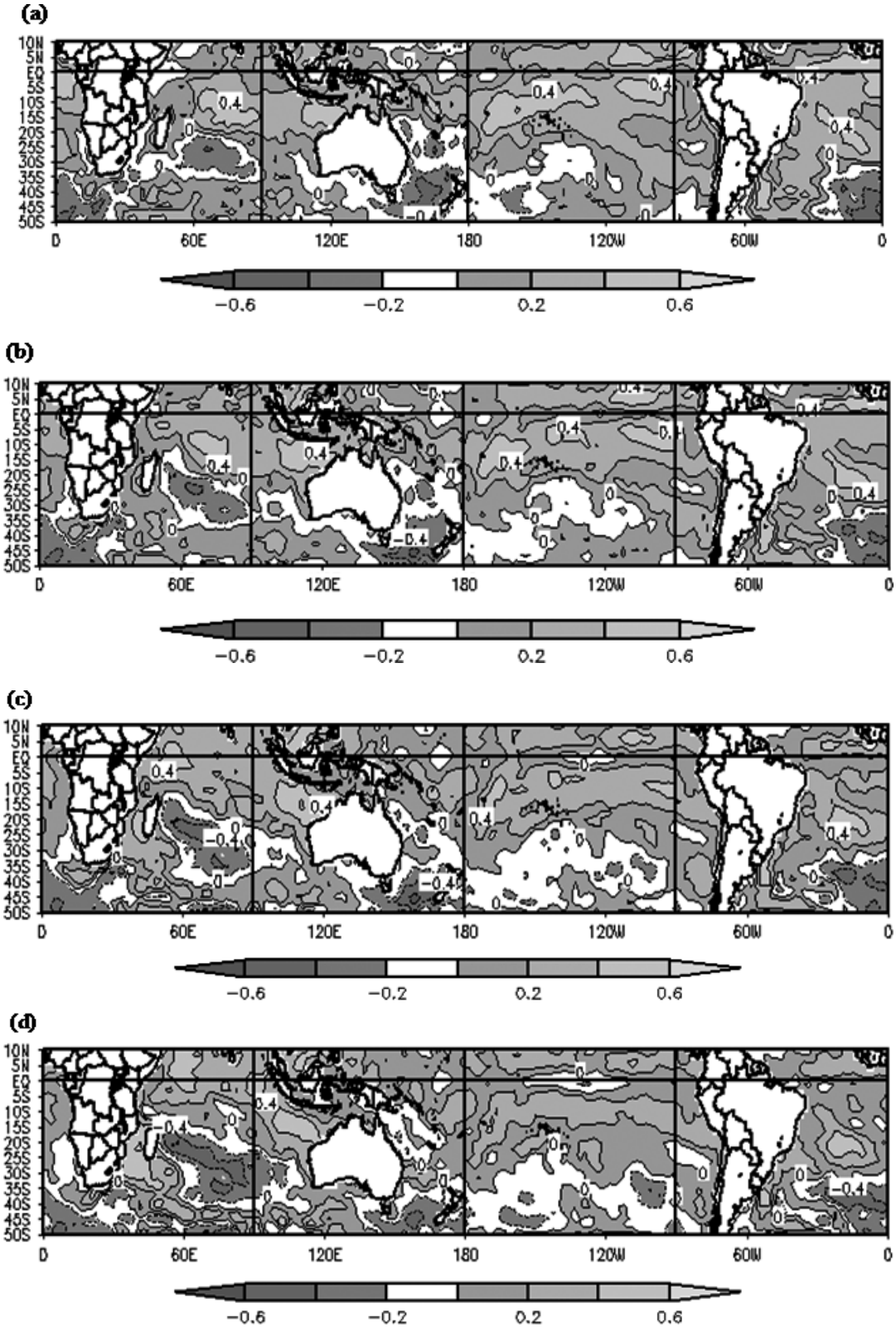

Figure 8. Lagged seasonal correlation between MJJ rainfall anomalies PC1 and (a) FMA, (b) MAM, (c) AMJ, and (d) MJJ sea surface temperature. Values larger than 0.4 correspond to those significant at 95% confidence level.

the largest relationship with PC1 in FMA. Moreover, the MJJ time series of PC2 is significantly correlated with the SST-IO index in the preceding FMA, while the correlation values for the next seasons subsequently decrease.

Table I confirms that PC4 is significantly related with both ENSO and SAM. While in FMA, SAM shows the largest correlation with PC4, during the next seasons both ENSO and SAM show similar correlation values. Accordingly, Silvestri and Vera (2003) described a combined

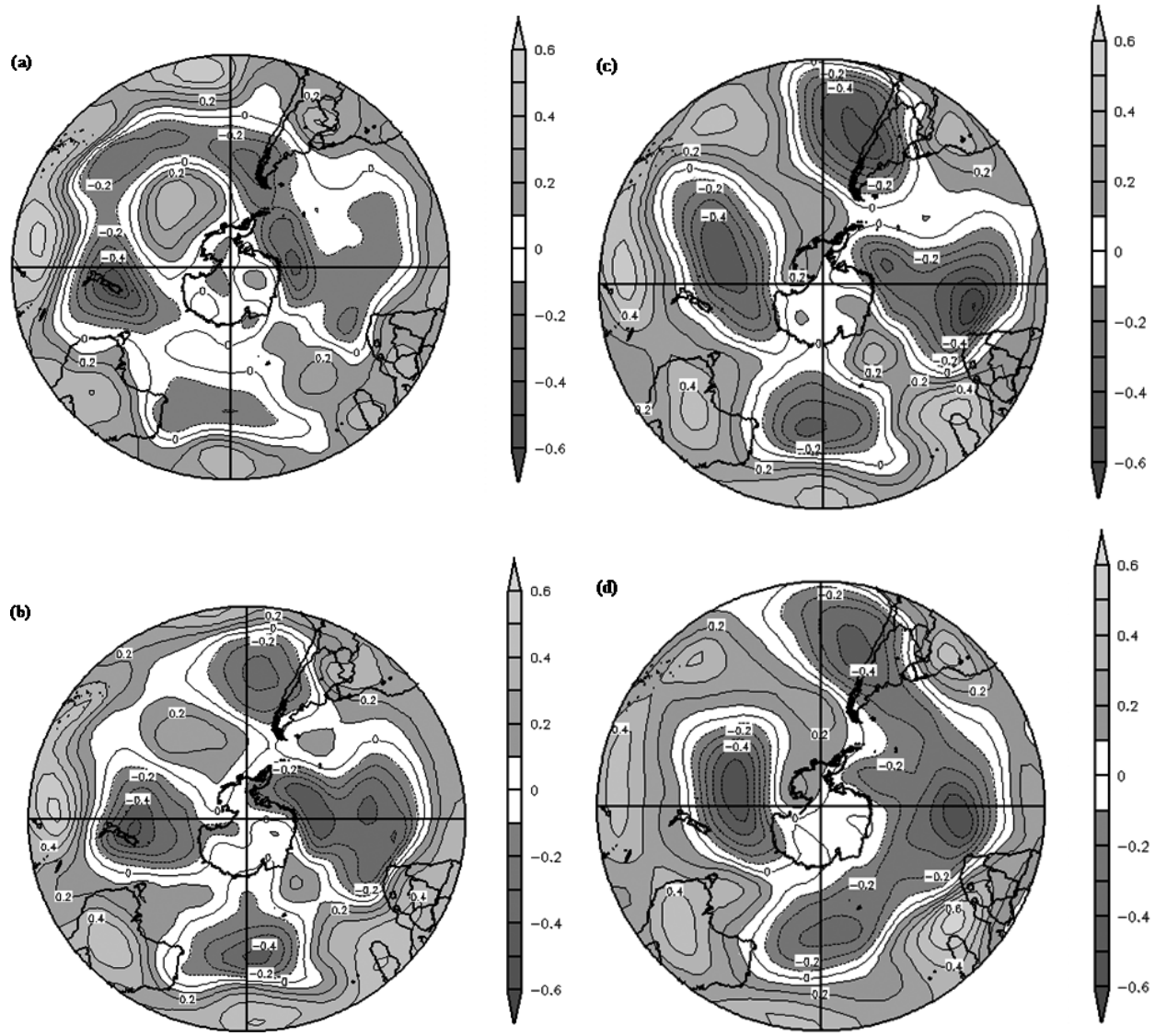

Figure 9. Lagged seasonal correlation between MJJ rainfall anomalies PC1 and (a) FMA, (b) MAM, (c) AMJ and (d) MJJ 500-hPa geopotential height. Values larger than 0.4 correspond to those significant at 95% confidence level.

Table I. Lagged correlations between the time series of PC1, PC2 and PC4 and the SST-IO, EN3.4 and AAO indexes (as defined in the text). Bolded (italic) numbers indicate statistically significant values at 90% (95%) confidence level.

	SST-IO			EN3.4			AAO		
	FMA	MAM	AMJ	FMA	MAM	AMJ	FMA	MAM	AMJ
PC1	−0.34	−0.26	−0.13	−0.26	−0.18	−0.09	0.07	0.02	0.12
PC2	***−0.46***	−0.24	−0.03	−0.02	0.11	0.18	−0.04	−0.01	0.06
PC4	−0.24	−0.33	−0.29	−0.37	**−0.43**	**−0.44**	***0.51***	**0.43**	**0.39**

influence of SAM and ENSO on the rainfall variability over southeastern South America.

6. Conclusions

This paper contributes to a better understanding of the main features associated with the rainfall interannual variability in a sector of the Southern Andes. The study was motivated by the fact that hydroelectric energy production and water availability in the area are highly sensitive to year-to-year changes in rainfall.

The analysis of the mean seasonal cycle shows that most of the rainfall occurs during winter, with maximum annual totals located over the Andes and decreasing eastwards. Three leading patterns essentially describe the spatial distribution of the regional rainfall interannual variability. PC1 and PC2 represent the variability over the southern and central part of the study region, respectively,

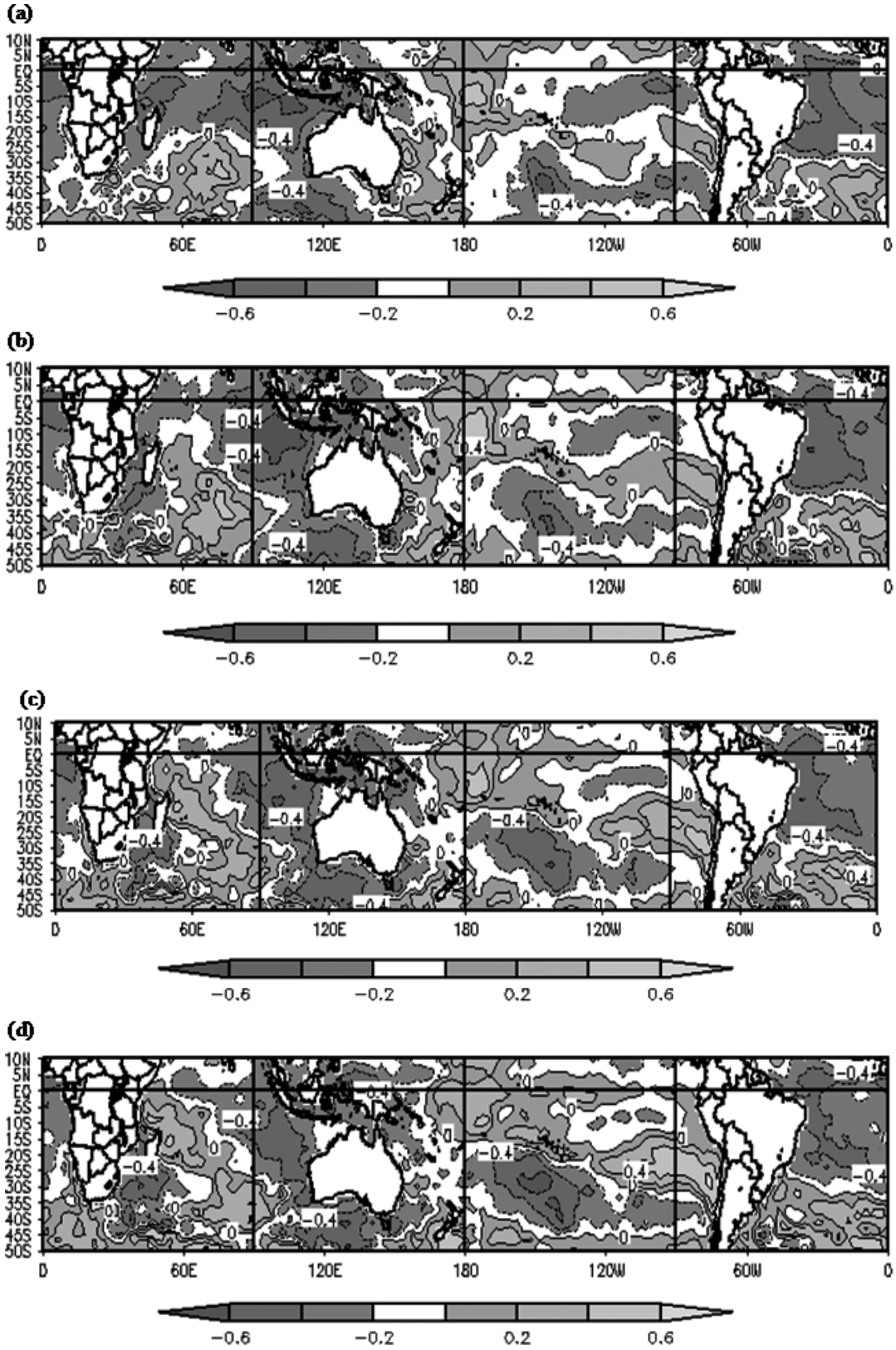

Figure 10. Same as in Figure 8 for PC2.

and exhibit considerable variability around 2 years. Low-level westerly anomalies are important in transporting moisture from the Pacific Ocean into the region. It was found that such westerly anomalies are promoted by regional circulation anomalies, which in turn are embedded in a large-scale wave train extending from Australia to South America. Furthermore, significant lagged correlations between the SST anomalies over the tropical Indian Ocean and the rainfall variability in the Southern Andes have been found. It is speculated

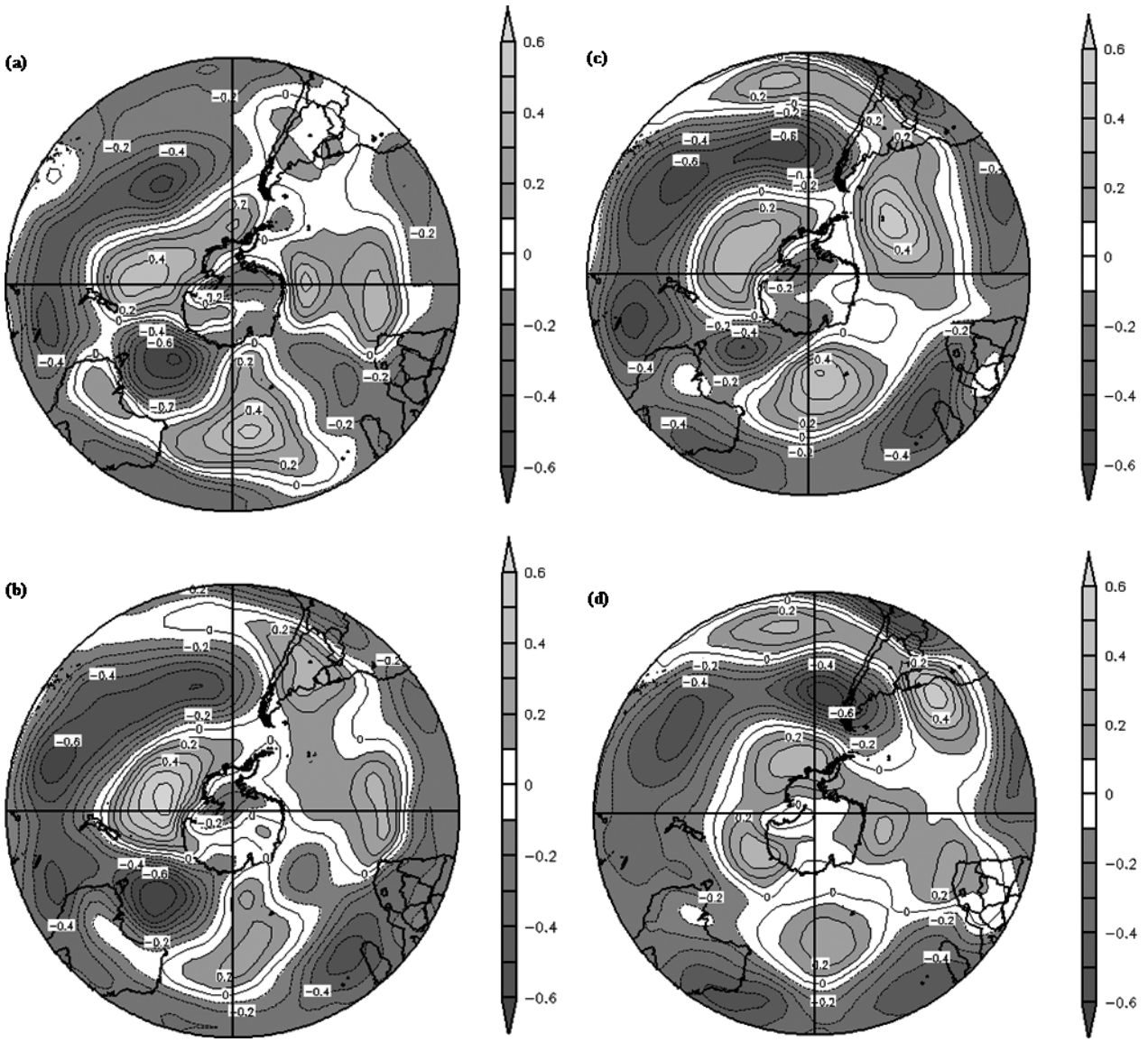

Figure 11. Same as in Figure 9 for PC2.

that such changes in the ocean surface conditions are responsible for inducing the Rossby wave train that extend along the South Pacific, between the tropical Indian Ocean and the region of interest.

In addition, PC4, which describes the rainfall variability in the northern portion of the region, shows a combined influence of ENSO and SAM. PC4 exhibits significant correlations with the SST anomalies in the central equatorial Pacific and with atmospheric circulation anomaly patterns associated with an annular-like structure at polar latitudes and a wave-like structure along the South Pacific.

The fact that changes in the conditions of both tropical Indian and Pacific Ocean significantly lead to the rainfall anomalies in the Southern Andes for at least a season provides some scope for seasonal prediction in the region. Previous works have pointed out the role of the tropical Indian Ocean conditions in influencing the large-scale circulation variability in the SH (Mo, 2000), and in particular the climate variability in the New Zealand region (Zheng and Frederiksen, 2006). Nevertheless, the Indian Ocean influence over the climate variability in extra-tropical South America and particularly over the Southern Andes regions has not been addressed yet. Therefore, the influence of the Indian Ocean conditions on the climate variability in the Southern Andes found in this work makes a significant and innovative contribution to the understanding of the sources of predictability in the region with relevant consequences for future applications on seasonal predictions.

Finally, it was found that SAM also exhibits linkages with the regional climate variability. Nevertheless, the fact that the SAM variability is dominant not only on interannual but also intraseasonal time scales and is essentially induced by the atmospheric internal variability might limit the skills of the regional seasonal prediction.

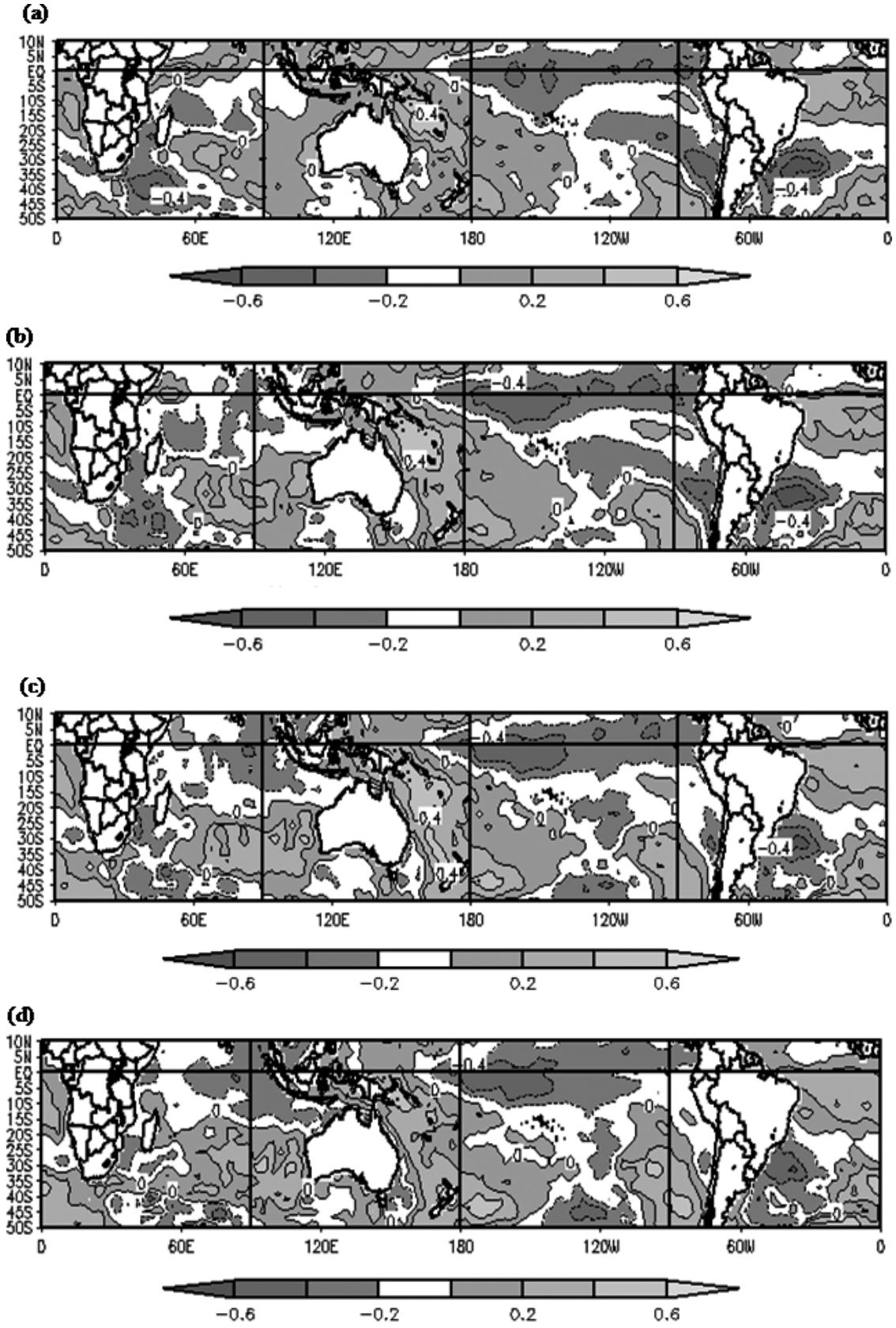

Figure 12. Same as in Figure 8 for PC4.

Acknowledgements

Images in Sections 3.3 and 3.4 were provided by the NOAA/ESRL Physical Sciences Division, Boulder Colorado, from their web site http://www.cdc.noaa.gov. This research was supported by UBA X444, UBA X160, CONICET PIP 5400, ANPCYT PICT04-25269 and PIP 112 - 200801 - 00195 CONICET.

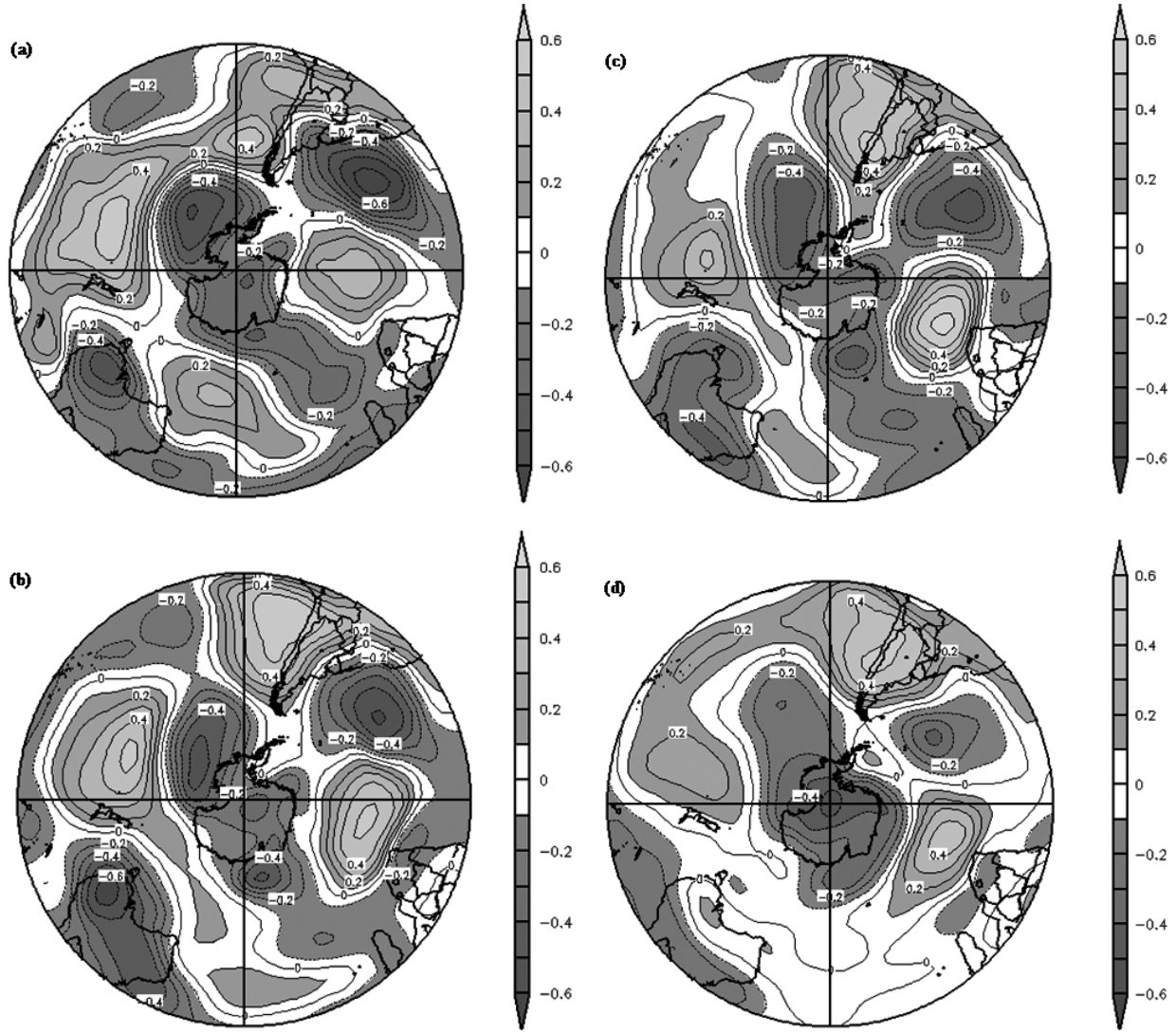

Figure 13. Same as in Figure 9 for PC4.

References

Aceituno P. 1988. On the functioning of the southern oscillation in the South American sector. Part I: surface climate. *Monthly Weather Review* **116**: 505–524.

Aceituno P, Garreaud R. 1995. Impactos de los fenómenos El Niño y La Niña sobre regímenes fluviométricos andinos. *Revista de la Sociedad Chilena de Ingenieria Hidráulica* **10**(2): 33–43.

Brooks C, Carruthers N. 1953. *Handbook of Statistical Methods in Meteorology*, Her Majesty's Stationary Office: London, UK; 210–241.

Cattel RB. 1966. The scree test for the number of factors. *Multivariate Behavioral Research* **1**: 245.

Compagnucci R, Araneo D. 2005. Identificación de áreas de homogeneidad estadística para los caudales de los ríos andinos argentinos y su relación con la circulación atmosférica y la temperatura superficial del mar. *Meteorologica* **30**(1,2): 41–54.

Compagnucci R, Vargas W. 1998. Inter-annual variability of the Cuyo river streamflowin the Argentinean Andean Mountains and ENSO events. *International Journal of Climatology* **18**: 1593–1609.

Conrad V, Pollack LW. 1950. *Methods in Climatology*, Harvard University Press: Cambridge, UK; 459.

Green P. 1978. *Analysing Multivariate Data*, Dryden Press: Illionis, USA; 341–387.

Hoffman J. 1975. Maps of mean temperature and precipitation. *Climatic Atlas of South America*, World Meteorol. Org.: Geneva, Switzerland; Vol. 1, 1–28.

Kaiser HF. 1958. The varimax criterion for analytic rotation in factor analysis. *Psychometrica* **23**: 187–200.

Kalnay E, Kanamitsu M, Kistler R, Collins W, Deaven D, Gandin L, Iredell M, Saha S, White G, Woollen J, Zhu I, Chelliah M, Ebisuzaki W, Higgings W, Janowiak J, Mo KC, Ropelewski C, Wang J, Leetmaa A, Reynolds R, Jenne R, Joseph D. 1996. The NCEP/NCAR Reanalysis 40 years-project. *Bulletin of the American Meteorological Society* **77**: 437–471.

Mo K. 2000. Relationships between low frequency variability in the southern hemisphere and sea surface temperature anomalies. *Journal of Climate* **13**: 3599–3610.

Montecinos A, Aceituno P. 2003. Seasonality of the ENSO related rainfall variability in central Chile and associated circulation anomalies. *Journal of Climate* **16**: 281–296.

Reason C. 2001. Subtropical Indian Ocean SST dipole events and Southern Africa rainfall. *Geophysical Research Letters* **28**: 2225–2227.

Reason C, Rouault M. 2005. Links between the Antartic Oscillation and winter rainfall over western South Africa. *Geophysical Research Letters* **32**: L07705. DOI: 10.1029/2005GL022419.

Routllant J, Fuenzalida H. 1991. Synoptic aspects of the central Chile rainfall variability associated with the southern oscillation. *International Journal of Climatology* **11**: 63–76.

Schneider C, Gies D. 2004. Effects of El Niño-Southern Oscillation on southernmost South America precipitation al 53 °S revealed from NCEP-NCAR reanalysis and weather station data. *International Journal of Climatology* **24**(9): 1057–1076.

Schwerdtfeger WS. 1975. *Climates of Central and South America*, *World Survey of Climatology*, Elsevier: Amsterdam; Vol. 12, 532.

Silvestri G, Vera C. 2003. Antarctic Oscillation signal on precipitation anomalies over southeastern South America. *Geophysical Research Letters*. **30**(21): 2115–2118, DOI: 10.1029/2003GL018277.

Thompson DWJ, Wallace JM. 2000. Annular modes in the extratropical circulation. Part I: Month-to-month variability. *Journal of Climate* **13**: 1000–1016.

Zheng X, Frederiksen C. 2006. A study of predictable patterns for seasonal forecasting of New Zealand rainfall. *Journal of Climate* **19**: 3320–3333.

Zheng X, Renwick J. 2003. A regression scheme based for seasonal forecasting of New Zealand temperature. *Journal of Climate* **16**: 1843–1853.

